

Hyperfine Stark effect of shallow donors in silicon

Giuseppe Pica,¹ Gary Wolfowicz,^{2,3} Matias Urdampilleta,² Mike L. W. Thewalt,⁴ Helge Riemann,⁵ Nikolai V. Abrosimov,⁵ Peter Becker,⁶ Hans-Joachim Pohl,⁷ John J. L. Morton,^{2,8} R. N. Bhatt,⁹ S. A. Lyon,⁹ and Brendon W. Lovett^{1,3}

¹*SUPA, School of Physics and Astronomy, University of St Andrews, KY16 9SS, United Kingdom*

²*London Centre for Nanotechnology, University College London, London WC1H 0AH, United Kingdom*

³*Dept. of Materials, Oxford University, Oxford OX1 3PH, United Kingdom*

⁴*Dept. of Physics, Simon Fraser University, Burnaby, British Columbia V5A 1S6, Canada*

⁵*Institute for Crystal Growth, Max-Born Strasse 2, D-12489 Berlin, Germany*

⁶*Physikalisch-Technische Bundesanstalt, D-38116 Braunschweig, Germany*

⁷*Vitcon Projectconsult GmbH, 07745 Jena, Germany*

⁸*Dept. of Electronic & Electrical Engineering, University College London, London WC1E 7JE, United Kingdom*

⁹*Dept. of Electrical Engineering, Princeton University, Princeton, New Jersey 08544, USA*

We present a complete theoretical treatment of Stark effects in doped silicon, whose predictions are supported by experimental measurements. A multi-valley effective mass theory, dealing non-perturbatively with valley-orbit interactions induced by a donor-dependent central cell potential, allows us to obtain a very reliable picture of the donor wave function within a relatively simple framework. Variational optimization of the $1s$ donor binding energies calculated with a new trial wave function, in a pseudopotential with two fitting parameters, allows an accurate match of the experimentally determined donor energy levels, while the correct limiting behavior for the electronic density, both close to and far from each impurity nucleus, is captured by fitting the measured contact hyperfine coupling between the donor nuclear and electron spin.

We go on to include an external uniform electric field in order to model Stark physics: With no extra *ad hoc* parameters, variational minimization of the complete donor ground energy allows a quantitative description of the field-induced reduction of electronic density at each impurity nucleus. Detailed comparisons with experimental values for the shifts of the contact hyperfine coupling reveal very close agreement for all the donors measured (P, As, Sb and Bi). Finally, we estimate field ionization thresholds for the donor ground states, thus setting upper limits to the gate manipulation times for single qubit operations in Kane-like architectures: the Si:Bi system is shown to allow for A gates as fast as ≈ 10 MHz.

I. INTRODUCTION

Donor spins in silicon represent one of the most promising and well studied candidates for quantum computing architectures¹. Very long coherence times have been measured in both nuclear² and electron spin donor qubits³, and individual spins can be manipulated and measured⁴⁻⁷. In any large scale information processing architecture, the application of an electric field is likely to be a vital enabling tool for addressing individual qubits⁸. Whatever the specific setting used, manipulation of quantum information in these systems requires a thorough understanding of how the energy levels of the spin qubits are modified by external magnetic or electric fields. These could either be deliberately applied to execute a particular gate operation, or exist anyway in an inhomogeneous electrostatic environment. Electric fields in particular can strongly affect two main properties of the donor via the Stark effect: the hyperfine coupling between the nuclear and the electron spin, proportional to the electronic density at the nuclear site, and the electron g -factor, i.e. the splitting induced by a magnetic field between the spin up and the spin down electronic levels.

Knowledge of such effects is ever more critical when an electric field is used to directly engineer the electronic wave function for storage or manipulation of quantum states^{1,8-11}. The first and most famous proposal of this kind was provided by Kane⁸, where a single qubit state, encoded in the impurity nuclear spin, is manipulated by using a Stark shift to bring it into resonance with an oscillating magnetic field. More

recently, scalable architectures have been proposed to extend single qubit control techniques to larger structures^{12,13}.

For these reasons, the Stark effect in doped silicon has been broadly studied in literature, either theoretically¹⁴⁻²¹ or experimentally²²⁻²⁵. More generally, the ability to theoretically describe the donor electron wave function accurately in a wide range of electrostatic environments is beneficial for determining the values of control parameters which provide best performance, and in the best case for estimating *a priori* the feasibility of quantum algorithms and error correction codes²⁰.

Nonetheless, the physical mechanisms underlying Stark effect of donors in silicon are not yet fully understood. The best attempt so far within effective mass theory (EMT) was proposed by Friesen¹⁵: For Si:P he correctly predicted a quadratic hyperfine shift, but one which is one order of magnitude larger than the value expected from the two measurements performed so far (Si:Sb²² and Si:As²³). More recently, other theories such as tight binding (TB) and Band Minima Basis (BMB)²¹ have been applied to the same Si:P problem, leading to closer agreement with experiment. TB and BMB, though, are computationally demanding numerical approaches, which eclipse full physical understanding. Current theoretical predictions of hyperfine shifts, then, are limited to Si:P alone, but other V group donors such as Bi are now established as promising alternative donor qubits and are being widely researched²⁶⁻³⁰. We are thus motivated to present a multi-valley EMT that provides a unifying framework for P, As, Sb and Bi donors. Theoretical predictions are supported by complete and precise

experimental work.

Finally, we will consider the effects of the electric field on the donor ground binding energy. This has raised opposing opinions^{15,18} as which of two competing effects play a dominant role in determining its magnitude: the lowering of single-valley energies due to admixing higher orbital states in the ground level, *vs* the narrowing of the valley-orbit $1s$ spectrum, which is a consequence of the reduced effect of the short-range impurity potential on the energy levels when the electron moves away from the nucleus. We clarify how the interplay of both results in an overall energy decrease of the ground donor state under the external field, confirming earlier *ab initio* calculations^{18,20}.

The highly successful match between our theory and experimental measurements motivates the determination of expected field ionization thresholds for each implanted donor species, setting *i*) upper limits to the achievable speeds for single-qubit operations relying on resonant excitation of selected donor electron spin transitions (like the Kane architecture⁸); and *ii*) gate voltages which should be applied to read-out the state of bulk qubits^{5,6}, possibly following transfer of quantum information to the electron spin from other degrees of freedom⁹.

II. THEORY

The Hamiltonian of a donor electron weakly bound to an impurity nucleus implanted in a silicon lattice is:

$$H\Psi(\mathbf{r}) = \left[-\frac{\hbar^2}{2m_0}\nabla^2 + V^0(\mathbf{r}) + U(\mathbf{r}) + e\mathbf{E}\cdot\mathbf{r} \right] \Psi(\mathbf{r}) = \epsilon\Psi(\mathbf{r}), \quad (1)$$

where $\Psi(\mathbf{r})$ is the wave function of the donor electron, m_0 is its rest mass, $V^0(\mathbf{r})$ is the periodic potential of the undoped silicon crystal, $U(\mathbf{r})$ accounts for the interaction with the impurity ion, \mathbf{E} is a uniform external electric field, and ϵ stands for the resulting energy eigenvalues.

The bottom conduction band in silicon has six equivalent minima (valleys) $\mathbf{k}_{0\mu}$, one along each of the crystallographic $\langle 100 \rangle$ directions in k space and located $\approx 86\%$ of the way to the edge of the Brillouin zone ($\mu = \pm x, \pm y, \pm z$). The donor ground state can be expanded to a good approximation in terms of packets of Bloch functions whose \mathbf{k} -vectors concentrate around each minimum. This is the cornerstone of EMT^{31,32}, which is improved further by accounting for the inter-valley coupling induced by the impurity potential. Such coupling is strongest in the lattice cell containing the donor nucleus – this is the so-called central cell correction^{33–36}. In this paper, we will use a multi-valley EMT which accounts for the anisotropy of the silicon conduction band and includes a suitable donor-dependent pseudopotential that mimics the impact of a dopant nucleus on the periodic environment of the undoped silicon lattice hosting the electron³³. Within the central cell, the impurity potential differs significantly from the screened Coulomb attraction usually considered in single valley-treatments^{31,32}, and is responsible for the lifting of the

valley degeneracy inherent to undoped silicon. We take:

$$U(\mathbf{r}) = -\frac{e^2}{\epsilon_{Si}|\mathbf{r}|}(1 - e^{-b|\mathbf{r}|} + B|\mathbf{r}|e^{-b|\mathbf{r}|}) \equiv -\frac{e^2}{\epsilon_{Si}|\mathbf{r}|} + U_{cc}(\mathbf{r}), \quad (2)$$

where $\epsilon_{Si} = 11.9$ is the static dielectric constant for silicon, e is the elementary charge, and b and B are parameters setting the two inverse lengthscales specific to the central cell corrections $U_{cc}(\mathbf{r})$ of each impurity potential.

After the usual EMT expansion in terms of the Si Bloch functions $\phi_0(\mathbf{k}, \mathbf{r}) \equiv u_0(\mathbf{k}, \mathbf{r})e^{i\mathbf{k}\cdot\mathbf{r}}$ with \mathbf{k} -vector close to each of the six $\mathbf{k}_{0\mu}$ ³¹, we have

$$\begin{aligned} \Psi(\mathbf{r}) &\equiv \sum_{\mu} \alpha_{\mu} \xi_{\mu}(\mathbf{r}) \\ &= \sum_{\mu} \alpha_{\mu} \frac{1}{(2\pi)^3} \int \tilde{F}_{\mu}(\mathbf{k}_{\mu} + \mathbf{k}_{0\mu}) \phi_0(\mathbf{k}_{\mu} + \mathbf{k}_{0\mu}, \mathbf{r}) d\mathbf{k}_{\mu}, \end{aligned} \quad (3)$$

with ξ_{μ} being the contribution of the envelope of Bloch functions centered at $\mathbf{k}_{0\mu}$. Following the other EMT approximations³⁶, the expectation value of Hamiltonian (1) for the wave function (3) is

$$\begin{aligned} \int d\mathbf{r} \sum_p \alpha_p^* F_p^*(\mathbf{r}) \times [\alpha_p(\mathbf{p}\cdot\mathbf{A}_i\cdot\mathbf{p} + e\mathbf{E}\cdot\mathbf{r} - \epsilon)F_p(\mathbf{r}) + \\ \sum_q \alpha_q e^{-i(\mathbf{k}_{0p}-\mathbf{k}_{0q})\cdot\mathbf{r}} C_0(\mathbf{k}_{0q}, \mathbf{k}_{0p})U(\mathbf{r})F_q(\mathbf{r})] = 0, \end{aligned} \quad (4)$$

where the sums over p and q are over the six valley minima; $\mathbf{p}\cdot\mathbf{A}_{\mu}\cdot\mathbf{p} \equiv T$ is the anisotropic kinetic energy operator, which implements the Hamiltonian of the undoped silicon lattice – first two terms in (1) – through two distinct effective masses ($m_{\perp}^* = 0.191m_0$ and $m_{\parallel}^* = 0.916m_0$), corresponding respectively to perpendicular and parallel motion with respect to each $\hat{\mu}$ axis. $C_0(\mathbf{k}_{0q}, \mathbf{k}_{0q}) = 1$, $C_0(\mathbf{k}_{0q}, \mathbf{k}_{0-q}) = -0.1728$ and $C_0(\mathbf{k}_{0q}, \mathbf{k}_{0\pm p}) = 0.4081(p \neq q)$, as further detailed in Ref. 37, are due to the lattice-periodic portion of the Bloch functions involved: $u_0^*(\mathbf{k}, \mathbf{r})u_0(\mathbf{k}', \mathbf{r}) = \sum_{\mathbf{G}} C_{\mathbf{G}}(\mathbf{k}, \mathbf{k}')e^{i\mathbf{G}\cdot\mathbf{r}}$ (where \mathbf{G} runs over the vectors of the silicon reciprocal lattice)³¹. In particular, EMT requires the Umklapp $\mathbf{G} \neq 0$ contributions to this product to be neglected.

A. Zero-field

With the external electric field turned off, we arbitrarily fix the two donor-dependent parameters of the pseudopotential (2), b and B , then variationally minimize the $1s$ -manifold energies

$$\epsilon_{1s} = \inf_{\Psi^{1s}} \{ \langle \Psi^{1s}(\mathbf{r}) | H | \Psi^{1s}(\mathbf{r}) \rangle : \langle \Psi^{1s}(\mathbf{r}) | \Psi^{1s}(\mathbf{r}) \rangle = 1 \}, \quad (5)$$

thus setting the corresponding optimal wave functions $\bar{\Psi}^{1s}$. The procedure is repeated with different values for b and B , until the experimental ionization energies of the singlet A_1 (the ground state), the triplet T_2 and the doublet E

Donor	b (nm ⁻¹)	B (nm ⁻¹)	$\epsilon_{A_1}^{exp}$ (meV) ⁴²	$\epsilon_{A_1}^{th}$ (meV)
P	8.55	37.06	-45.59	-45.75
As	17.74	136.84	-53.76	-53.54
Sb	33.58	386.44	-42.74	-42.92
Bi	48.46	1055.7	-70.98	-71.08

TABLE I: Pseudopotential parameters b and B as defined in Eq. 2 for various V group donors leading to best agreement of the theoretical ground energy $\epsilon_{A_1}^{th}$ with its experimental counterpart $\epsilon_{A_1}^{exp}$.

eigenstates are reproduced. Those states are the result of the lifting of the six-fold aforementioned valley degeneracy, and their coefficients $\{\alpha_q\}$ (see Eq. 3) are fixed by tetrahedral symmetry³⁸, consistent with the pseudopotential employed here.

Previous multi-valley EMT studies^{33,35,36,39} have also employed a variational approach, but with hydrogenic Bohr functions as trial effective mass envelopes $F_q(\mathbf{r})$, to compute the same energy levels. While the variational method is expected to give reliable guesses at the binding energies, no rigorous inferences can be drawn about the exact nature of the wave function: this is the reason why many different pseudopotentials and EMT approximations used in the past led to satisfactory agreement with the former, but poor descriptions of the latter. As a first improvement, in a previous paper³⁷ we highlighted the importance of using anisotropic envelopes and imposing further constraints on the shape of the wave function, as indicated by experimental measurements. More precisely, we set the trial ground state function of a Si:P electron to match the experimental contact hyperfine coupling, which is proportional to the value of the electron density at the impurity site.

When trying to extend the same approach to include donors other than P, however, we found that matching both binding energies and hyperfine coupling at the same time cannot be satisfied for Sb and Bi: more strongly non-isocoric donors (i.e. those that are more different from the hosting silicon atoms)³⁴ display a larger contact hyperfine coupling, and are expected to need a more careful account of the central cell corrections. Nonetheless, the single-valley limit is a trustworthy solution far enough from the nucleus³¹, where the screened Coulomb interaction represents a good approximation to the potential felt by the effective mass electron. For those donors, anisotropic Bohr envelopes are too simple to mediate between those contrasting features. We highlight here how more accurate pictures of the electronic spatial density, both close to and far from the nuclear region, can be achieved if envelopes with more structure are used to describe the donor wave function. Two different pairs of anisotropic Bohr radii that distinguish the short (a_s, b_s) from the long (a_l, b_l) range hydrogen-like decay, and a relative weight β of the two parts,

Donor	A_0 (MHz) ⁴⁰	$ \Psi(0) _{exp}^2$ (cm ⁻³) ⁴⁰	$ \Psi(0) _{th}^2$ (cm ⁻³)
P	117.53	0.43×10^{24}	0.46×10^{24}
As	198.35	1.73×10^{24}	1.78×10^{24}
Sb	186.80	1.18×10^{24}	1.15×10^{24}
Bi	1475.4	1.4×10^{25}	1.4×10^{25}

TABLE II: Theoretical values are calculated as $|\Psi(0)|_{th}^2 = 6\eta|F^0(0)|^2$, where $\eta = |u_0(\mathbf{k}_0, 0)|^2 / |u_0(\mathbf{k}_0, \mathbf{r})|_{\text{unit cell}}^2 = 159.4$ is taken from Ref. 41, and F^0 is either envelope in Eq. 6.

define our trial envelopes:

$$\begin{aligned} F_z^0 &= N_0 \left[e^{-\sqrt{\frac{x^2+y^2}{a_s^2} + \frac{z^2}{b_s^2}}} + \beta e^{-\sqrt{\frac{x^2+y^2}{a_l^2} + \frac{z^2}{b_l^2}}}, \right. \\ F_x^0 &= N_0 \left[e^{-\sqrt{\frac{z^2+y^2}{a_s^2} + \frac{x^2}{b_s^2}}} + \beta e^{-\sqrt{\frac{z^2+y^2}{a_l^2} + \frac{x^2}{b_l^2}}}, \right. \end{aligned} \quad (6)$$

where N_0 is a normalization factor. When looking for the optimal solutions in Eq. (5), a_s, b_s are essentially fixed by the central cell potential (i.e. they depend strongly on b and B), while β, a_l, b_l set the resultant long-distance tail, which depends on the screened Coulomb potential surviving further from the nucleus.

This approach is inspired by the observation that, even with only one valley [e.g. setting $\alpha_1 = 1, \alpha_q = 0$ if $q \neq 1$ in Eq. (4)], the Hamiltonian to be solved is that of a screened hydrogen atom with an extra short range potential, hence the principal quantum number n which labels the radial eigenfunctions of the hydrogen atom is not an exact quantum number for the s states. Anisotropic exponentially decaying shapes are known to provide reliable solutions for a Coulomb-bound electron with two different effective masses along orthogonal spatial directions (see parameters a_l, b_l above)³¹, and the nature of the central cell potential in Eq. (2) suggests the same *ansatz* for the (a_s, b_s) part³³.

The pseudopotential values that fit $1s$ energies and hyperfine coupling for each donor are reported in Table I, alongside the relative ground state energies; expected electronic densities at the nuclear site are listed in Table II, together with the corresponding values deducible from measurements⁴⁰. The optimal parameters which characterize all ground wave functions, and are used to calculate theoretical values in Tables I and II, are listed in Table III.

B. Field on

The solution of the problem of a hydrogen atom in vacuum within a uniform external electric field \mathbf{E} (the Stark effect) has long been known⁴³. Perturbation theory correctly predicts, for small fields, quadratic shifts of the ground state energy, linear terms in $|\mathbf{E}| \equiv E$ being prevented by parity symmetry. The curvature can only be calculated precisely, though, after an infinite sum over all excited orbital states is admixed into $1s$.

Donor	\bar{a}_s (nm)	\bar{b}_s (nm)	$\bar{\beta}$	\bar{a}_l (nm)	\bar{b}_l (nm)
P	0.303	0.181	0.92285	1.71	0.912
As	0.192	0.114	0.47403	1.45	0.737
Sb	0.146	0.0852	0.47289	1.67	0.889
Bi	0.0968	0.0572	0.27153	0.967	0.472

TABLE III: Wave function parameters for the donor ground state as defined in Eq. (6), found by variational minimization as shown in Eq. (5). All long-range radii \bar{a}_l, \bar{b}_l are significantly smaller than the Kohn-Luttinger values $a_{\text{KL}} = 2.365$ nm, $b_{\text{KL}} = 1.36$ nm³¹, due to central-cell corrections. Though Si:Sb is more non-isocoric than Si:P, their wave functions look similar in the region far from the nucleus, in line with their similar ground binding energies.

An alternative approach is supplied by variational theory: the *ansatz* for the ground state under a uniform electric field⁴⁴ is inspired by the first order perturbative correction to the wave function:

$$\psi(\mathbf{r}) = [1 + (q_1 + q_2 r)z]e^{-r/a_B}, \quad (7)$$

with a_B the Bohr radius, $r = \sqrt{x^2 + y^2 + z^2}$, while the variational coefficients q_1 and q_2 represent the weight of higher orbital states coupled to the fundamental one, and are determined via the principle of minimization of the binding energy of the state in Eq. (7).

The Stark effect in vacuum is complicated, in the framework of shallow donor states in silicon, by two factors: *i*) as shown in the previous paragraph, the zero-field potential felt by the donor electron, has a short-ranged impurity potential component on top of the (screened) Coulomb interaction. This modifies the response to the field of each separate valley as treated within a single-valley approach, so these are termed *intra-valley corrections*; *ii*) the non-trivial structure of the silicon conduction band introduces the extra valley degree of freedom, hence it becomes important to account for the rearranging of the *inter-valley interactions* under $E \neq 0$. Our multi-valley EMT provides one of the most straightforward schemes that can capture the interplay between those two features, and also leads to physical insight.⁴⁸

Following these considerations, our trial zero-field envelopes (6) are modified as¹⁵

$$\begin{aligned} F_z &= N_z \left[e^{-\sqrt{\frac{x^2+y^2}{a_s^2} + \frac{z^2}{b_s^2}}} + \beta e^{-\sqrt{\frac{x^2+y^2}{a_{l,z}^2} + \frac{z^2}{b_{l,z}^2}}} \right] (1 + q_z z), \\ F_x &= N_x \left[e^{-\sqrt{\frac{z^2+y^2}{a_s^2} + \frac{x^2}{b_s^2}}} + \beta e^{-\sqrt{\frac{z^2+y^2}{a_{l,x}^2} + \frac{x^2}{b_{l,x}^2}}} \right] (1 + q_x z), \end{aligned} \quad (8)$$

with $q_x, q_z, a_{l,x}, b_{l,x}, a_{l,z}, b_{l,z}$ being variational parameters, as we justify later on. This procedure is expected to give an appropriate account of the adjustment of each valley to the altered electrostatic environment. Another novelty of our theory is that, for each fixed \mathbf{E} value, we choose to minimize the complete singlet A_1 ground energy, noting that at $\mathbf{E} = 0$ this is a symmetric superposition of all valleys ($\alpha_\mu = 1/\sqrt{6} \forall \mu$ in Eq. 3). Earlier works^{15,44} have optimized the binding energy relative to each valley alone. This is a

crucial step forward that allows us to treat valley-orbit effects in a non-perturbative way, and to depict consistently how they are modified by inhomogeneous potentials.

Let us write the Hamiltonian above in matrix form, in the valley basis $\{\xi_\mu\}$. If we assume, with no loss of generality, that $\mathbf{E} \parallel \hat{\mathbf{z}}$ ¹⁵, we have:

$$H = \begin{pmatrix} \Lambda_x & \Delta_{1x} & \Delta_{2xy} & \Delta_{2xy} & \Delta_{2xz} & \Delta_{2xz} \\ \Delta_{1x} & \Lambda_x & \Delta_{2xy} & \Delta_{2xy} & \Delta_{2xz} & \Delta_{2xz} \\ \Delta_{2xy} & \Delta_{2xy} & \Lambda_x & \Delta_{1x} & \Delta_{2xz} & \Delta_{2xz} \\ \Delta_{2xy} & \Delta_{2xy} & \Delta_{1x} & \Lambda_x & \Delta_{2xz} & \Delta_{2xz} \\ \Delta_{2xz} & \Delta_{2xz} & \Delta_{2xz} & \Delta_{2xz} & \Lambda_z & \Delta_{1z} \\ \Delta_{2xz} & \Delta_{2xz} & \Delta_{2xz} & \Delta_{2xz} & \Delta_{1z} & \Lambda_z \end{pmatrix} \quad (9)$$

where $H_{\mu\nu} = \langle \xi_\mu | H | \xi_\nu \rangle$. Diagonal entries Λ_μ correspond to intra-valley energies, while $\Delta_{1\mu}, \Delta_{2\mu\nu}$ terms represent couplings between $(\xi_\mu, \xi_{-\mu})$ and (ξ_μ, ξ_ν) respectively. After diagonalization, the ground eigenvector and eigenenergy are simple functions of those matrix elements¹⁵:

$$\begin{aligned} \epsilon_g &= \frac{1}{2} \left(\Lambda_x + \Lambda_z + \Delta_{1x} + \Delta_{1z} + 2\Delta_{2xy} \right. \\ &\quad \left. + \sqrt{32\Delta_{2xz}^2 + (\Lambda_x - \Lambda_z + \Delta_{1x} - \Delta_{1z} + 2\Delta_{2xy})^2} \right), \end{aligned} \quad (10)$$

and

$$\{\alpha_\mu\}_g = \frac{(1, 1, 1, 1, \gamma, \gamma)}{\sqrt{4 + 2\gamma^2}}, \quad (11)$$

where

$$\begin{aligned} \gamma &= \frac{1}{4\Delta_{2xz}} \left[-(\Lambda_x - \Lambda_z + \Delta_{1x} - \Delta_{1z} + 2\Delta_{2xy}) \right. \\ &\quad \left. + \sqrt{32\Delta_{2xz}^2 + (\Lambda_x - \Lambda_z + \Delta_{1x} - \Delta_{1z} + 2\Delta_{2xy})^2} \right]. \end{aligned} \quad (12)$$

It will be appreciated that our matrix is different from that appearing in Friesen's theory of Stark effect¹⁵ for four reasons: we consider the whole Bloch functions including the lattice-periodic part, rather than the plane-wave part alone; central cell corrections are implemented in a self-consistent way, fit to experimental electronic properties and crafted to coincide with expected limiting behaviours of the wave

function; Eq. (4) does not involve spurious inter-valley coupling induced by the kinetic portion of the Hamiltonian, in contrast with Twose's equation³⁹; and, finally, our envelopes are not approximated by their amplitude at the impurity site (a constant), since our $U_{cc}(\mathbf{r})$ in Eq. (2) is not a contact potential.

As the effective local electric field due to $U_{cc}(\mathbf{r})$ is always much larger in the region close to the nucleus than the external one due to the field (for the parameter regime considered here), the variational parameters of the donor envelopes in Eq. (8) that pertain to that region are not affected significantly by the field. On the contrary, the long range radii a_l, b_l and the coefficients q_x, q_z , representing the 'squeezing' of the wave function in the z direction, encode all the Stark sensitivity of the ground state Ψ^{1s} . Distinct a_l, b_l are allowed for the envelopes $F_{\pm z}$ in the direction of the field, and for the transverse ones $F_{\pm x}, F_{\pm y}$, as they are expected to adjust differently to the $\mathbf{E} \parallel \hat{\mathbf{z}}$ perturbation. For each fixed E , the optimal values \bar{q}_x, \bar{q}_z and $\bar{a}_{l,x}, \bar{b}_{l,x}, \bar{a}_{l,z}, \bar{b}_{l,z}$, that minimize ϵ_g , fix all matrix elements in Eq. (9), whence γ and $\{\alpha_\mu\}_g$ are consequently determined.

Deviations of $\Lambda_{x,z}$ from the zero-field values $\Lambda_{x,z}^0$ are seen to be respectively one and two orders of magnitude larger than those of the off-diagonal $\Delta_{2\mu\nu}$ and $\Delta_{1\mu}$ in (9). These inter-valley terms get negligible alterations from the field directly, since higher Fourier components of a linear Hamiltonian potential $\propto Ez$ are not able to couple significantly different valleys: they only change due to the weak squeezing of the envelopes of each separate valley in the z direction. Hence, after expansion of Eq. (10) up to second order in the field, it is possible to approximate

$$\epsilon_g - \epsilon_g^0 \approx \frac{1}{3}(\Lambda_x - \Lambda_z), \quad (13)$$

$$\gamma \approx 1 - \frac{1}{6} \frac{\Lambda_x - \Lambda_z}{\Delta_{2xz}}. \quad (14)$$

If we consider the differential equations that lead to the optimal solution in more detail, we can distinguish different trends within the parameter space, as a function of the field. Since $q_x a_l (q_z b_l) \ll 1$ (i.e. the amount of the squeezing of the envelopes in the z direction $\langle F_{x(z)}(\mathbf{r}) | z | F_{x(z)}(\mathbf{r}) \rangle$ is very small compared to their zero-field spatial extent), to an excellent degree of approximation

$$\begin{aligned} \Lambda_x &\equiv \Lambda_x^0 + \Delta\Lambda_x \\ &\approx \Lambda_x^0 + q_x^2 \langle F_x^0 | z | (-\Lambda_x^0 + T + U(\mathbf{r})) | z F_x^0 \rangle \\ &\quad + eE q_x \langle F_x^0 | z^2 | F_x^0 \rangle. \end{aligned} \quad (15)$$

(The same expressions and discussions presented for the x valleys hold for the z ones, changing $x \rightarrow z$ in the subscripts). Since clearly Λ_x^0 does not depend on q_x , the equation $0 = \partial\epsilon_g/\partial q_x \propto \partial\Lambda_x/\partial q_x$, which determines \bar{q}_x , decouples from all others and gives

$$2\bar{q}_x = - \frac{eE \langle F_x^0 | z^2 | F_x^0 \rangle}{\langle F_x^0 | z | (-\Lambda_x^0 + T + U(\mathbf{r})) | z F_x^0 \rangle}. \quad (16)$$

As the denominator is positive, it must be that \bar{q}_x, \bar{q}_z are negative, and their magnitude increases linearly with the field.

The wave function extends further along the z axis, in the opposite direction to the vector field \mathbf{E} (Fig. 1). This accounts for admixture into the fundamental wave function of p and higher angular momentum orbitals, with the correct singlet A_1 valley-structure⁴⁹.

We find, on the other hand, that the radii a_l, b_l undergo a slight shift from their zero-field values, only to adjust to the new energy terms $\Delta\Lambda_{x,z}$ in Eq. (15). Specifically, the differential equations determining the optimized radii $\bar{a}_{l,x}, \bar{b}_{l,x}, \bar{a}_{l,z}, \bar{b}_{l,z}$ have the form

$$\begin{aligned} \epsilon_g^0 [a_l^0 \rightarrow \{a_{l,x}, a_{l,z}\}, a_l^0 \rightarrow \{b_{l,x}, b_{l,z}\}] - \epsilon_g^0 + \\ \Delta\epsilon_g [a_l^0 \rightarrow \{a_{l,x}, a_{l,z}\}, a_l^0 \rightarrow \{b_{l,x}, b_{l,z}\}] = 0, \end{aligned} \quad (17)$$

where $a_l^0 \rightarrow \{a_{l,x}, a_{l,z}\}$ is a shorthand for variations $a_l^0 \rightarrow a_{l,x}(a_{l,z})$ within each envelope $F_x(F_z)$. The first row is only second order in $\delta a_l, \delta b_l$ (the unperturbed energy is stationary against small changes of the wave function), while the second includes linear terms in $\delta a_l, \delta b_l$. Thus, the total shifts of the intra-valley energies Λ_μ [and consequently of the total ϵ_g , via Eq. (13)] is due to the parameters \bar{q}_x, \bar{q}_z alone:

$$\Delta\Lambda_{x,z} \approx eE \langle F_{x,z}(\mathbf{r}) | z | F_{x,z}(\mathbf{r}) \rangle / 2 \sim \bar{q}_{x,z} E \sim E^2, \quad (18)$$

leading immediately, considering Eq. (13) and (14), to $\epsilon_g - \epsilon_g^0 \propto E^2, (\gamma - 1) \propto E^2$. It then follows that $\{\delta a_l, \delta b_l\} \propto \{\bar{q}_x, \bar{q}_z\} E \propto E^2$: these small variations of radii play a decisive role in determining the relative fraction of electronic density leftover at the impurity site, which allows the correct estimates of the Stark shifts presented here.

Let us highlight that, due to the silicon transverse effective mass m_\perp^* being smaller than the longitudinal m_\parallel^* , F_x extends more broadly in the z direction than F_z , hence in Eq. (18) $|\Delta\Lambda_x| > |\Delta\Lambda_z|$: the valleys transverse to the applied perturbation react more effectively than the parallel ones, and this observation will have important consequences, as will become clear when we present our results later on.

III. HYPERFINE STARK SHIFT

The hyperfine interaction between the electron spin \mathbf{S} and the nuclear spin \mathbf{I} is described though a coupling tensor \mathbf{A}

$$H_{\text{HF}} = \mathbf{I} \cdot \mathbf{A} \cdot \mathbf{S}. \quad (19)$$

The most relevant part of H_{HF} , which is usually exploited in quantum computing schemes, is the Fermi contact scalar term $A \mathbf{I} \cdot \mathbf{S}^8$, whose values we listed in Table II for all four group V donors. ESR and NMR donor spectra are determined primarily by the interplay between hyperfine and Zeeman splittings, which can result in non-trivial dependence of spin transition frequencies on the background magnetic field B , with interesting applications in single qubit control²⁷. Such features have been exploited in numerous proposals, with successful experimental realizations already achieved in some cases^{28,30,45}. In particular, the ability to tune these resonant frequencies with external electrostatic gates has often been exploited in proposals^{9,10}. In the presence of a modified

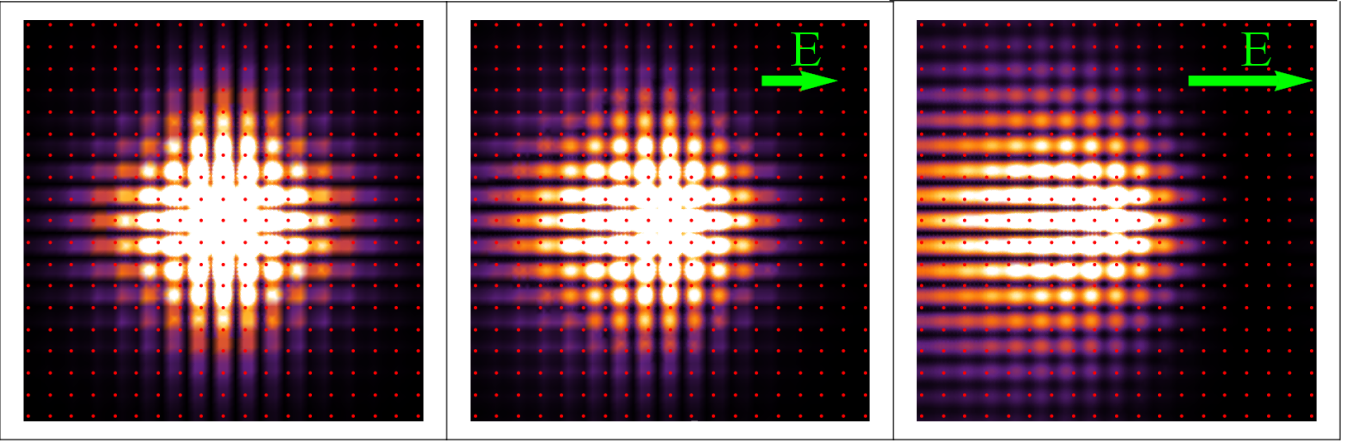


FIG. 1: Spatial electronic density of a Si:P bulk donor electron around the implanted nucleus it is bound to, in the plane (010), up to 5 nm away from donor nucleus along the vertical and the horizontal axes. The three panels show how the density changes under different electrostatic environments: The left panel shows the symmetric situation for the isotropic $\mathbf{E} = 0$ case, the center and the right panel display how the density is driven off the central nucleus in the direction opposite to the vector \mathbf{E} , under an intermediate and a strong electric field, respectively. Red dots represent the positions of the silicon nuclei of the underlying lattice: their positions do not coincide with the local maxima and minima of the density because of the interference of different valleys contributing to the ground state wave function.

electrostatic environment, the electronic density can be pulled off the impurity site, and thus the hyperfine coupling can be altered. The pertinent regime for quantum computing schemes, and which will also be explored by measurements reported in the Sec. IV, is one of weak fields – of order a few tenths of a $V/\mu\text{m}$, which is well below ionization threshold⁸. As stated previously, in this regime we expect a quadratic dependence on E :

$$\frac{\Delta A}{A_0} \equiv \frac{|\Psi(\mathbf{E} \neq 0, \mathbf{r} = 0)|^2}{|\Psi(\mathbf{E} = 0, \mathbf{r} = 0)|^2} - 1 \equiv \eta_a E^2. \quad (20)$$

Unlike ϵ_g , the coefficient η_a is significantly influenced by the precise value of the long range radii \bar{a}_l, \bar{b}_l :

$$\eta_a = \left(\frac{1}{6F^0(\mathbf{0})^2} \frac{4}{4 + 2\gamma^2} [2F_x(E, \mathbf{0}) + \gamma F_z(E, \mathbf{0})]^2 - 1 \right) \frac{1}{E^2}, \quad (21)$$

where $F^0(\mathbf{0})$ is the value of any zero-field envelope evaluated at the nuclear site. γ depends on E^2 , but much more weakly, hence it can be effectively considered equal to 1 for the evaluations of ΔA below.

The optimal parameters enter Eq. (21) essentially through the normalizations $N_x = \langle F_x | F_x \rangle, N_z = \langle F_z | F_z \rangle$, since $F_{x(z)}(\mathbf{0}) = N_{x(z)}(1 + \beta)$ [see Eq. (8)]. Let us highlight the two ways ΔA depends quadratically on E : From Eqs. (20) and (21)

$$\Delta A = \frac{1}{9} \left(2 \frac{N_x}{N_0} + \frac{N_z}{N_0} \right)^2 - 1, \quad (22)$$

where $i) N_x(N_z) \propto q_x^2(q_z^2) \propto E^2$ (for parity symmetry reasons, N_x and N_z cannot comprise linear terms in \bar{q}_x, \bar{q}_z , being expectation values of the identity, an even operator); $ii)$ to lowest order, $(N_{x(z)}/N_0 - 1) \approx$

Donor	$\eta_a(\mu\text{m}^2/V^2)$ (th)	$\eta_a(\mu\text{m}^2/V^2)$ (exp)
P	-3.0×10^{-3}	$-(2.5 \pm 0.5) \times 10^{-3}$
As	-1.2×10^{-3}	$-(1.2 \pm 0.1) \times 10^{-3}$
Sb	-3.7×10^{-3}	$-(3.5 \pm 0.05) \times 10^{-3}$
Bi	-0.16×10^{-3}	$-(0.26 \pm 0.05) \times 10^{-3}$

TABLE IV: Quadratic Stark shift coefficients η_a (th) of the hyperfine couplings of four group V donors in silicon, as calculated from Eq. (21), and compared to respective experimental values η_a (exp) found in Sec. IV. As we discuss in Sec. IV, the P, As and Sb donors are measured in the same sample and so here we quote only errors relative to one another; there is an additional absolute error of about 17% of the shift which is plotted in Fig. 3

$\frac{1}{N_0} \left(\frac{\partial N_0}{\partial a_l} \delta a_{l,x(z)} + \frac{\partial N_0}{\partial b_l} \delta b_{l,x(z)} \right)$, then from the discussion at the end of the previous section we know $\{\delta a_l, \delta b_l\} \propto E^2$.

Hyperfine frequency shifts for each donor are displayed as a function of applied field in Fig. 2. From least-squares fitting of those graphs, we obtain values for the quadratic Stark shift coefficient η_a of hyperfine couplings of all donors considered here; these are shown in Table IV, alongside their respective experimental values, which have been measured for this study to high precision as will be detailed in Sec. IV.

The agreement is excellent for P, As and Sb, and good for Bi; the latter is very non-isocoric³⁴, thus an effective mass treatment is expected to work not as well. More specifically, the Umklapp valley-orbit terms neglected in Eq. (4) are more important, and the EMT approximations are less justified. Nonetheless, the Stark shift of Bi is still correctly found to be the lowest of the V group donors.

Let us stress that the ordering of the magnitudes of η_a coefficients across different donors, i.e. the trend in the tendency of the corresponding electron to be pulled off the nucleus, follows the pattern suggested by the donors' binding

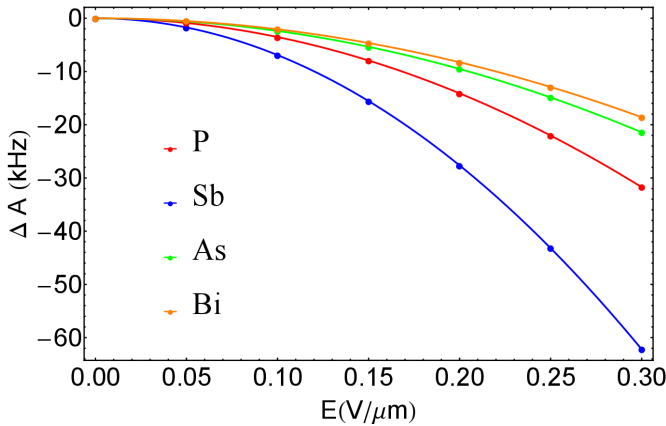


FIG. 2: Absolute hyperfine frequency shifts ΔA as calculated from Eq. (21), as a function of the applied uniform field E , for all donors considered here. The field range shown is typical of those required for executing quantum gates and corresponds to the range investigated experimentally in Sec. IV, but is well below the ionization thresholds discussed in Sec. V.

energies, rather than being dictated by the respective hyperfine couplings as one may naively expect. This is shown in Fig. 3, where both theoretical and experimental η_a coefficients are reported, for all donors, in correspondence to their respective ground binding energies. Specifically, Si:Sb shows the largest η_a since it is the shallowest of all donors, and in spite of the fact that it has a stronger A_0 than Si:P (see Table II). In other words, it does not only matter how concentrated the electron is at the nuclear site – more important is how much the ground state is spread further from the impurity,. This can be deduced from Eq.(16), (and a similar expression for \bar{q}_z) where all the quantities involved are expectation values on the state $|F^0 z\rangle$, which has vanishing amplitude around $z \approx 0$.

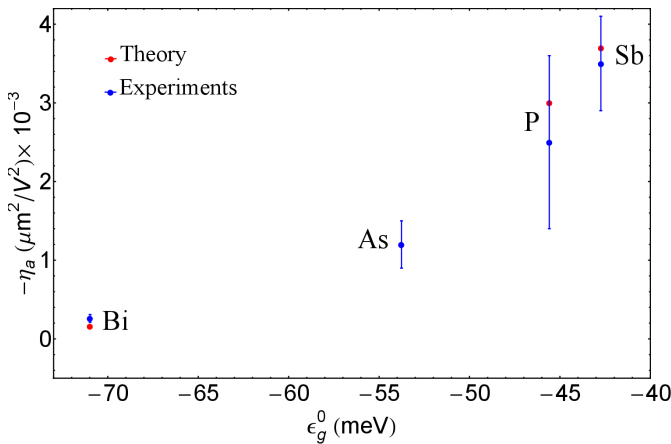


FIG. 3: Donor η_a coefficients as a function of the zero-field ground binding energy ϵ_g^0 : Both theoretical points (red) and experimental values with absolute errors (blue) are reported. The monotonic dependence displayed here is qualitatively explained in the text. The predicted and the measured η_a coefficient of Si:As overlap with each other.

IV. EXPERIMENTAL METHODS

Stark shift experiments were performed on ensembles of spins for the four group V donors in two different samples. Material 1 contains ^{31}P , ^{75}As and ^{121}Sb donors ranging in concentration between 10^{14} and 10^{15} cm^{-3} . Material 2 has Bi in concentration of $2 \times 10^{15} \text{ cm}^{-3}$. Both materials are isotopically purified silicon-28 float-zone crystals with below 100 ppm isotope concentration of ^{29}Si and ^{30}Si . The measurements were realized in a pulse electron spin resonance (ESR) X-band (0.3 T, 9.7 GHz) Bruker spectrometer at temperatures ranging from 5 to 11 K; for each donor, the temperature is adjusted so that the electron spin-lattice relaxation $T_{1e} \approx 30 - 40 \text{ ms}$). Samples of materials 1 and 2 are sandwiched between two metallic plates in between which the voltage is applied, to generate the field in a parallel plate capacitor configuration.

Owing to the Stark effect, the electric field shifts the ESR frequency which can then be measured as a phase shift over time (see Fig. 4(b)). The frequency shift can be directly retrieved by Fourier-transforming (F.T.) this phase acquisition (see Fig. 4). Then the frequency shift for all ESR transitions of the four donors can be measured at different electric fields, see Fig. 5. The sensitivity of the measurement is thus limited by the frequency deviation and the acquisition time (limited by T_{2e}). The electric field deviation, $\sigma_E/\langle E \rangle$, is typically around 15%, since the plates are not perfectly parallel due to samples geometry and roughness, and the acquisition time can be made as long as 1.6 ms by using a dynamical decoupling sequence (see Fig. 4(a)). Experimental errors such as variation in sample thickness, voltage pulse rise and set times have also been taken into account. Finally, because P, As and Sb were measured on the same sample of material 1, in exactly the same configuration, the errors in Table IV are only given relative to one another, taking into account only the fit error from Fig. 5. Due the above mentioned inhomogeneities, there is an additional absolute error of about 17% of these η_a values, which were calculated by Monte Carlo sampling over all frequency (F.T.) distributions. This additional error is not included in Table IV but is shown in Fig. 3.

Local strain or charge defects in the sample create an internal electric field E_{in} . In the presence of an external electric field E_{ex} , the Stark shift is:

$$\Delta f \propto (E_{ex} + E_{in})^2 = 2E_{in}E_{ex} + E_{in}^2 + E_{ex}^2. \quad (23)$$

As a result, the defect induced Stark shift has a component that depends linearly on the external electric field²². This component is expected to be strictly inhomogeneous and thus results in a decay of the electron spin echo signal - but it can be cancelled by applying bipolar (positive and negative) electric pulses, as given by the sequence depicted on Fig. 4(a). The quadratic shift which we want to measure is still acquired under this sequence.

The Stark-induced frequency (f) shift combines both the hyperfine (A) and the spin-orbit (g) contributions. They both depend quadratically on the applied electric field, but the sensitivity of the frequency to each of them (df/dA and df/dg , respectively) depends on both the nuclear state

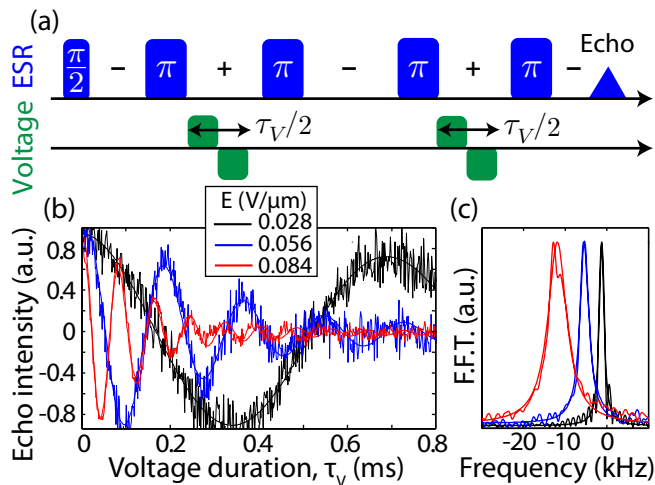


FIG. 4: Measurement of the Stark shift in $^{28}\text{Si}:^{121}\text{Sb}$ using dynamical decoupling. (a) Uhrig Dynamical Decoupling (UDD) sequence with four refocusing pulses. As each π pulse reverses the phase acquisition (see signs in sequence), the DC electric field is applied in between alternating pairs of π pulses. Using positive and negative voltage pulses, the linear Stark shift contribution, arising from local defects, is eliminated and only the quadratic part remains. (b) Electron spin phase evolution measured in the $m_I = +5/2$ ESR transition of Sb in material 1 for different electric fields. (c) Fast Fourier-transform (F.F.T) showing the frequency shift distribution in the sample, fitted here with a Lorentzian fit.

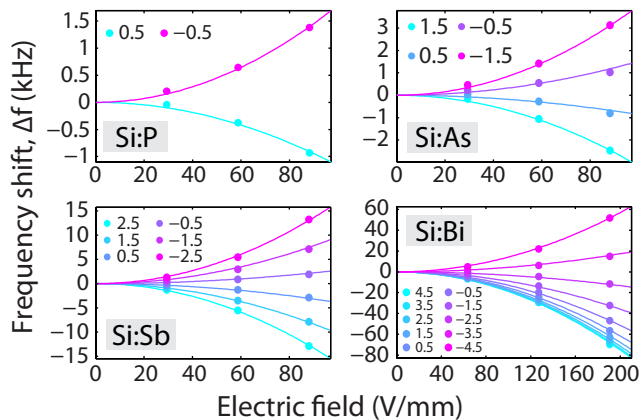


FIG. 5: Stark shift for P, As, Sb and Bi measured at X-band, for each possible ESR transitions. The quadratic η_a and η_g shift coefficients are the only parameters in the fits (lines). (a) ^{31}P , (b) ^{75}As , (c) ^{121}Sb and (d) ^{209}Bi .

m_I and the magnetic field B_0 . In the high field limit (no mixing) and for the electron spin transition, $df/dA = m_I$ and $df/dg = \mu_B B_0$. For $B_0 < 1$ T, the hyperfine contribution is then expected to be strongly dominant over the spin-orbit contribution. Thus, at X-band, measuring the Stark shift for each of the m_I states provides a good estimate of the hyperfine contribution in very good agreement with theoretical values (see Fig. 3). The values of η_a measured here agree well with previous results for As and Sb^{22,23}, while this is the first time

they have been reported for P and Bi.

V. GROUND STATE ENERGY AND ELECTRON IONIZATION

Using our previous analysis, captured by Eq. (13), and keeping in mind that $\Lambda_x < \Lambda_z < 0$, we find that the absolute magnitude of the donor binding energy $|\epsilon_g|$ increases with increasing field. This is non-trivial behaviour that arises from the combination of effects discussed in Sec. II, where we saw how the lowering of intra-valley energies produced by the field, see Eq. (18), is the only important factor in determining the change in the total donor binding energy with E . The impact on the shape of the wave function in the central-cell region modifies ϵ_g negligibly, hence the inter-valley interactions are not affected significantly, and the spectral narrowing of the $1s$ manifold is not strong enough to produce an overall energy increase of the ground state. Our conclusion contrasts with Ref. 15, where the electron was predicted to be less bound in increasing field, but it confirms the conclusions in the *ab initio* treatments presented in Refs. 18,20.

We find the dependence of the ground state energy on the field is rather weak, as shown in the $1s A_1$ energy plots of Fig. 6: this is compatible with studies performed within different approaches²⁰, and confirms that bulk donor electrons ‘instantaneously’ tunnel off an impurity nucleus, in contrast to adiabatic tuning available to electrons closer to an interface¹⁴.

So far we have dealt with electric fields of magnitudes that would be required for the execution of quantum gate operations. As E increases by one order of magnitude above those considered so far, qualitatively new dynamics takes place¹⁸: the $2p$ -like orbital levels of the donor electron (with the singlet A_1 valley structure) anti-cross with the slowly changing ground $1s$ -like state, so that the electron can effectively tunnel off the bulk of the silicon layer. Using our model we can predict the ionization field for each of the donor chemical species. The size of this field is important, since spin dependent tunnelling is a leading proposed read-out technique for solid state spins^{7,9}. Such read-out often occurs at the interface with an oxide layer, or close to an SET device^{5,6}, which is rather far from the dopant nucleus and thus requires ionization of the donor electron.

We compute the Stark shifted binding energy of the bulk A_1 ‘ $2p_0$ ’ state as a function of the field (see Fig. 6), by variational optimization of Hamiltonian (1) on the following trial wave function:

$$\Psi^{2p}(\mathbf{r}) = N_p z e^{-\sqrt{\frac{x^2+y^2}{a_p^2} + \frac{z^2}{b_p^2}} (1 + q_z^p z), \quad (24)$$

which is suggested by the zero-field form in Ref. 32, modified to include the admixing with higher energy states induced by the applied external field. Let us remark that valley-orbit effects play practically no role in determining the energy and the wave function of this state (and more generally, of all non- s states), since the corresponding orbital is concentrated far from the impurity nucleus and is thus not sensitive to the

non-Coulombic potential $U_{cc}(\mathbf{r})$. For the same reason, its features do not depend on the specific chemical donor species.

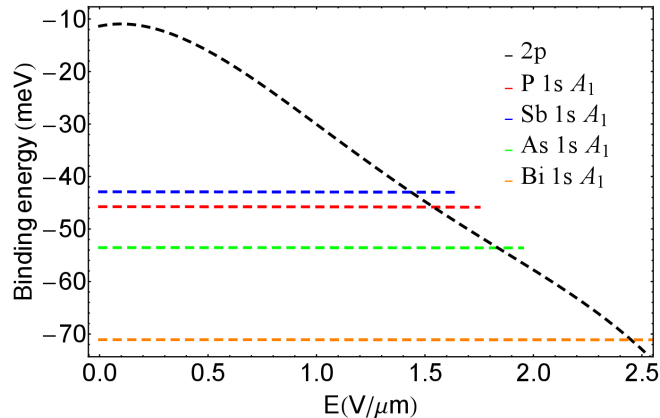


FIG. 6: Donor binding energies of the ground states of Si:P, Si:Sb, Si:As, and Si:Bi decrease very weakly as a function of the field, as detailed in the text. For each species, values are reported only up to the point E_c where they become degenerate with the ‘ $2p$ ’ energy level, which is common to all donors, as it is not influenced by central cell corrections. Each crossing point corresponds to the ionizing field for each donor.

We stress that the energy levels shown in Fig. 6 refer to the diagonal Hamiltonian terms $\langle \Psi^{2p} | H | \Psi^{2p} \rangle$ and $\langle \Psi^{1s} | H | \Psi^{1s} \rangle$, i.e. we do not take into account the off-diagonal couplings $\langle \Psi^{2p} | H | \Psi^{1s} \rangle$. The latter would lead to the expected anti-crossing of the levels as hybridization between Ψ^{1s} and Ψ^{2p} occurs. However, the field at which $\langle \Psi^{2p} | H | \Psi^{2p} \rangle = \langle \Psi^{1s} | H | \Psi^{1s} \rangle$ provides a good estimate of the ionization field E_c ⁴⁶.

The dependence of the A_1 $2p$ binding energy on field qualitatively confirms the behavior calculated in Refs. 14,18 and 20 for a donor electron state closer than 25 nm to the interface with a dioxide. Our results are specific to impurities implanted deep in the bulk of a Si layer, though, and hence there are quantitative differences of a few tenths of $V/\mu\text{m}$ between our results and the threshold for Si:P and Si:As predicted in those references. We report in Table V, for the first time, the expected ionization fields for all bulk donors.

While specific measurements of these thresholds are still lacking, very recent experimental work²³ reports that Si:As donor electrons are ionized at $E \sim 2 V/\mu\text{m}$, in full agreement with our prediction.

Other than identifying precise field regimes that are relevant for bulk donor spin read-out, our study allows us to extract another piece of information valuable to any silicon quantum computing scheme. Single qubit operations in this system are performed via selective microwave (ESR) magnetic pulses addressing the hyperfine- and Zeeman-split transitions of the donor electron spin levels (in the high magnetic field limit, electron-spin levels are only weakly hyperfine-mixed with the nuclear spin ones, i.e. the electron spin projection m_S is a good quantum number). In order to manipulate individual spins within a large ensemble of implanted donors it is easiest⁴⁷ to apply a global alternating magnetic field

Donor	Ionization field E_c (V/ μm)	Maximum hyperfine shift ΔA^{max} (MHz)	Maximum ESR frequency shift Δf^{max} (MHz)
P	1.55	0.8	0.4
As	1.84	0.8	1.2
Sb	1.45	1.4	3.5
Bi	2.45	1.4 (2.1)	6.3 (9.5)

TABLE V: Predictions of the size of the electric field required to ionize each donor species, and the corresponding maximum absolute hyperfine shift ΔA^{max} that can be achieved before the electron tunnels away from the nucleus. Each ESR frequency shift $\Delta f^{max} = \Delta A^{max} m_I$ in the last column are for a nuclear magnetic moment $m_I = I$ (i.e. the maximum possible value of m_I) and represents the largest transition frequency shift that can be induced by the applied field E with each donor. The first ΔA^{max} , Δf^{max} for Bi are calculated using the theoretical value for η_a given in Table IV, while the bracketed value refers to the experimental η_a measured here and available in Table IV.

B_{ac} , bringing only selected qubits in resonance with it, by locally Stark-shifting their spin-resonance frequency⁸. The selected ESR transitions can be shifted by at most $\Delta f(E) = \eta_a E^2 A_0 m_I$ with m_I , the nuclear spin projection, equal to the nuclear spin quantum number I ⁴⁵. This maximum shift sets the limit on how quickly spins can be manipulated: if the timescale τ of B_{ac} pulses is shorter than Δf^{-1} , then the resonance frequencies of the non-selected qubits will lie within the pulse bandwidth. It follows that faster gates can be performed with larger Δf , and this is in turn limited by the ionization threshold presented here.

We estimate the maximum hyperfine frequency shifts that donor ESR transitions can undergo in silicon while still being safe from ionization: results are reported in Table V. Si:Bi supports gate times as short as $\Delta f_{max}^{-1} \sim 100$ ns, yielding the fastest manipulation obtainable with Kane-like A gates⁸ within donor spins systems in silicon.

VI. CONCLUSIONS

Our theory provides the first comprehensive treatment of Stark effects for donors in silicon. The inherent physical mechanisms behind them are unveiled by the analytic and insightful multi-valley EMT framework. After appropriate calibration using bulk donor properties, we obtain an excellent match with experimental hyperfine shifts of all V group donors under a non-zero applied electric field. The reported measurements of hyperfine Stark shifts include the first experimental hyperfine η_a coefficient of Si:P and Si:Bi.

We establish that the donor electron is slightly more bound to the nucleus with an increasing field, for small fields, and calculate field thresholds at which ionization is expected to occur, for each donor. This leads us to estimating the maximum frequency shifts of ESR transitions that can be achieved by A gates in a Kane-like architecture. Very short operation times, as fast as ~ 100 ns, are allowed if the qubit

is implemented in the Si:Bi electron spin.

Building on these results, our reliable wave functions are ready to be used for calculation of other single and two donor electron properties, especially those relevant for implementing quantum information processing protocols. They represent a fast and flexible scheme rich in physical insight, easily extendable to include more complicated electromagnetic environments, such as interfaces, non-uniform electric fields, and hybrid donor-dot schemes.

VII. ACKNOWLEDGEMENTS

We thank C.C. Lo and A.M. Tyryshkin for valuable discussions. This research was funded by the joint EPSRC (EP/I035536) / NSF (DMR-1107606) Materials

World Network grant (BWL, GP, JJLM, SAL), EPSRC grant EP/K025562/1 (BWL and JJLM), the European Research Council under the European Community's Seventh Framework Programme (FP7/2007-2013) / ERC grant agreement no. 279781 (JJLM), partly by the NSF MRSEC grant DMR-0819860 (SAL), the Department of Energy, Office of Basic Energy Sciences grant de-sc0002140 (RNB). BWL and JJLM thank the Royal Society for a University Research Fellowship. RNB thanks the School of Natural Sciences, Institute for Advanced Study, Princeton for hospitality during the period when this work was done. The 28-Si-enriched samples used in this study were prepared from Avo28 material produced by the International Avogadro Coordination (IAC) Project (2004-2011) in cooperation among the BIPM, the IN-RIM (Italy), the IRMM (EU), the NMIA (Australia), the NMIJ (Japan), the NPL (UK), and the PTB (Germany).

- ¹ F. A. Zwanenburg, A. S. Dzurak, A. Morello, M. Y. Simmons, L. C. L. Hollenberg, G. Klimeck, S. Rogge, S. N. Coppersmith, and M. A. Eriksson, *Rev. Mod. Phys.* **85**, 961 (2013).
- ² K. Saeedi, S. Simmons, J. Z. Salvail, P. Dluhy, H. Riemann, N. V. Abrosimov, P. Becker, H.-J. Pohl, J. J. L. Morton, and M. L. W. Thewalt, *Science* **342**, 830 (2013).
- ³ A. M. Tyryshkin, S. Tojo, J. J. L. Morton, H. Riemann, N. V. Abrosimov, P. Becker, H.-J. Pohl, T. Schenkel, M. L. W. Thewalt, K. M. Itoh, et al., *Nat. Mater.* **11**, 143 (2012).
- ⁴ A. Morello, J. J. Pla, F. A. Zwanenburg, K. W. Chan, K. Y. Tan, H. Huebl, M. Mottonen, C. D. Nugroho, C. Y. Yang, J. A. van Donkelaar, et al., *Nature* **467**, 687 (2010).
- ⁵ J. J. Pla, K. Y. Tan, J. P. Dehollain, W. H. Lim, J. J. L. Morton, F. A. Zwanenburg, D. N. Jamieson, A. S. Dzurak, and A. Morello, *Nature* **496**, 334 (2013).
- ⁶ J. J. Pla, K. Y. Tan, J. P. Dehollain, W. H. Lim, J. J. L. Morton, D. N. Jamieson, A. S. Dzurak, and A. Morello, *Nature* **489**, 541 (2012).
- ⁷ D.R. McCamey, J. Van Tol, G. W. Morley, and C. Boehme, *Science* **330**, 1652 (2010).
- ⁸ B. E. Kane, *Nature* **393**, 133 (1998).
- ⁹ J. J. L. Morton, A. M. Tyryshkin, R. M. Brown, S. Shankar, B. W. Lovett, A. Ardavan, T. Schenkel, E. E. Haller, J. W. Ager, and S. A. Lyon, *Nature* **455**, 1085 (2008).
- ¹⁰ G.P. Lansbergen, R. Rahman, C.J. Wellard, I. Woo, J. Caro, N. Collaert, S. Biesemans, G. Klimeck, L.C.L. Hollenberg and S. Rogge, *Nature Physics* **4**, 656 (2008).
- ¹¹ J. Verduijn, G. C. Tettamanzi, and S. Rogge, *Nano Letters* **13**, 1476 (2013).
- ¹² H. Büch, S. Mahapatra, R. Rahman, M.Y. Simmons, A. Morello, *Nature Communications* **4**, 2017 (2013).
- ¹³ R. Kalra, A. Laucht, C.D. Hill, and A. Morello, *Phys. Rev. X* **4**, 021044 (2014).
- ¹⁴ A. S. Martins, R. B. Capaz, and B. Koiller, *Phys. Rev. B* **69**, 085320 (2004).
- ¹⁵ M. Friesen, *Phys. Rev. Lett.* **94**, 186403 (2005).
- ¹⁶ C. J. Wellard, L. C. L. Hollenberg, and C. I. Pakes, *Nanotechnology* **13**, 570 (2002).
- ¹⁷ A. De, C. E. Pryor, and M. E. Flatté, *Phys. Rev. Lett.* **102**, 017603 (2009).
- ¹⁸ A. Debernardi, A. Baldereschi, and M. Fanciulli, *Phys. Rev. B* **74**, 035202 (2006).
- ¹⁹ L. Pendo, E. M. Handberg, V. N. Smelyanskiy, and A. G. Petukhov, *Phys. Rev. B* **88**, 045307 (2013).
- ²⁰ R. Rahman, G. P. Lansbergen, S. H. Park, J. Verduijn, G. Klimeck, S. Rogge, and L. C. L. Hollenberg, *Phys. Rev. B* **80**, 165314 (2009).
- ²¹ R. Rahman, C. J. Wellard, F. R. Bradbury, M. Prada, J. H. Cole, G. Klimeck, and L. C. L. Hollenberg, *Phys. Rev. Lett.* **99**, 036403 (2007).
- ²² F. R. Bradbury, A. M. Tyryshkin, G. Sabouret, J. Bokor, T. Schenkel, and S. A. Lyon, *Phys. Rev. Lett.* **97**, 176404 (2006).
- ²³ C. C. Lo, S. Simmons, R. Lo Nardo, C. D. Weis, A. M. Tyryshkin, J. Meijer, D. Rogalla, S. A. Lyon, J. Bokor, T. Schenkel, and J. J. L. Morton, *Appl. Phys. Lett.* **104**, 193502 (2014).
- ²⁴ G. D. Watkins and F. S. Ham, *Phys. Rev. B* **1**, 4071 (1970).
- ²⁵ D. K. Wilson and G. Feher, *Phys. Rev.* **124**, 1068 (1961).
- ²⁶ R. E. George, W. Witzel, H. Riemann, N. V. Abrosimov, N. Nötzel, M. L. W. Thewalt and J. J. L. Morton, *Phys. Rev. Lett.* **105**, 067601 (2010).
- ²⁷ G. Wolfowicz, A.M. Tyryshkin, R.E. George, H. Riemann, N.V. Abrosimov, P. Becker, H.J. Pohl, M.L.W. Thewalt, S.A. Lyon, J.J.L. Morton, *Nature Nanotechnology* **8**, 561 (2013).
- ²⁸ M. H. Mohammady, G. W. Morley, and T. S. Monteiro, *Phys. Rev. Lett.* **105**, 067602 (2010).
- ²⁹ C. D. Weis, C. C. Lo, V. Lang, A. M. Tyryshkin, R. E. George, K. M. Yu, J. Bokor, S. A. Lyon, J. J. L. Morton, and T. Schenkel, *Applied Physics Letters* **100**, 172104 (2012).
- ³⁰ G.W. Morley, M. Warner, A.M. Stoneham, P.T. Greenland, J. van Tol, C.W.M. Kay, G. Aeppli, *Nature Materials* **9**, 725 (2010).
- ³¹ W. Kohn and J. M. Luttinger, *Phys. Rev.* **98**, 915 (1955).
- ³² J. M. Luttinger and W. Kohn, *Phys. Rev.* **97**, 869 (1955).
- ³³ T. H. Ning and C. T. Sah, *Phys. Rev. B* **4**, 3482 (1971).
- ³⁴ S.T. Pantelides and C. T. Sah, *Phys. Rev. B* **10**, 621 (1974).
- ³⁵ K. Shindo and H. Nara, *J. Phys. Soc. Jpn.* **40**, 1640 (1976).
- ³⁶ H. T. Hui, *Solid State Commun.* **154**, 19 (2013).
- ³⁷ G. Pica, B. W. Lovett, R. N. Bhatt, and S. A. Lyon, *Phys. Rev. B* **89**, 235306 (2014).
- ³⁸ W. Kohn, *Solid State Physics*, vol. 5 (Academic Press, 2010).
- ³⁹ H. Fritzsche, *Phys. Rev.* **125**, 1560 (1962).
- ⁴⁰ G. Feher, *Phys. Rev.* **103**, 834 (1956).
- ⁴¹ L. V. C. Assali, H. M. Petrilli, R. B. Capaz, B. Koiller, X. Hu, and

- S. Das Sarma, Phys. Rev. B **83**, 165301 (2011).
- ⁴² A. K. Ramdas and S. Rodriguez, Reports on Progress in Physics **44**, 1297 (1981).
- ⁴³ H. Friedrich, *Theoretical Atomic Physics* (Springer-Verlag,1990).
- ⁴⁴ L. Pendo, E. M. Handberg, V. N. Smelyanskiy, and A. G. Petukhov, Phys. Rev. B **88**, 045307 (2013).
- ⁴⁵ G. Wolfowicz, M. Urdampilleta, M.L.W. Thewalt, H. Riemann, N.V. Abrosimov, P. Becker, H.J Pohl, and J. J. L. Morton, arXiv Prepr., 1, (2014), arXiv:1405.7420.
- ⁴⁶ M. J. Calderon, B. Koiller, and S. Das Sarma, Phys. Rev. B **75**, 125311 (2007).
- ⁴⁷ J. J.L. Morton, D. R. McCamey, M. A. Eriksson, and S. A. Lyon, Nature **479**, 345 (2011).
- ⁴⁸ We assume in the following, within EMT approximations, that the field dependence of the wave function is entirely ascribed to the envelope part of $\Psi(\mathbf{r})$, i.e. we do not include the adjustment of the periodic part of the Bloch functions.
- ⁴⁹ The field cannot couple the ground state to other s -like orbitals, due to parity symmetry; nor to high angular momentum states which have orthogonal valley structures T_2 and E .